research papers

A Shack–Hartmann measuring head for the two-dimensional characterization of X-ray mirrors

Johan Floriot,[a]* Xavier Levecq,[a] Samuel Bucourt,[a] Muriel Thomasset,[b] François Polack,[b] Mourad Idir,[b] Pascal Mercère,[b] Thierry Moreno[b] and Sylvain Brochet[b]

[a]Imagine Optic, France, and [b]Synchrotron Soleil, France. E-mail: jfloriot@imagine-optic.com

The recent development of short-wavelength optics (X/EUV, synchrotrons) requires improved metrology techniques in terms of accuracy and curvature dynamic range. In this article a stitching Shack–Hartmann head dedicated to be mounted on translation stages for the characterization of X-ray mirrors is presented. The principle of the instrument is described and experimental results for an X-ray toroidal mirror are presented. Submicroradian performances can be achieved and systematic comparison with a classical long-trace profiler is presented. The accuracy and wide dynamic range of the Shack–Hartmann long-trace-profiler head allow two-dimensional characterizations of surface figure and curvature with a submillimeter spatial resolution.

1. Introduction

The progress of short-wavelength optics (X/EUV and synchrotron applications) calls for optical components with higher and higher surface figure. Consequently, the characterization of such high-quality components requires improved metrology techniques in terms of accuracy and curvature dynamic range (in order to be able to measure radii of curvature <1 m). X-ray mirrors are always used in grazing incidence because performing the total reflection condition requires grazing angles of the order of 1–100 mrad, as the refraction index of materials in this spectral domain is very close to 1 ($n = 1 - \delta$, where δ is of the order of 10^{-4} to 10^{-3} for wavelengths around 1 nm). Consequently, their profile is rectangular and their dimensions are typically 100–1500 mm along the tangential direction and 20–100 mm along the sagittal one. Moreover, such mirrors can show very highly curved shapes in the sagittal direction (spherical, cylindrical or toroidal with very small radii of curvature) for X-ray beam collimation or focalization (in a Kirkpatrick–Baez configuration, for example).

Manufacturers generally characterize X-ray mirrors with interferometers. These instruments allow the characterization of plane and spherical surfaces for a large range of radius of curvature (provided that gauge surfaces are available to produce stable and high-quality reference wavefronts). On the other hand, synchrotron users often use long-trace profilers (LTPs) (Thomasset *et al.*, 2005) in order to characterize the optics before their installation on beamlines. LTPs do not need

a reference wavefront but their curvature dynamic range is limited. Moreover, both interferometers and LTPs are subject to vibrations and thermal drifts so that a careful control of the experimental conditions is required. Alternative techniques such as Shack–Hartmann wavefront sensing have recently emerged for the nanotopographic characterization of Si wafers. This technique benefits from the robustness of the Shack–Hartmann technology (insensitivity to vibrations, simple design) and can achieve equivalent performances as interferometers without the need of reference wavefronts. As the aperture of the instrument is much smaller than the dimensions of the surface under test, mappings are performed using translation stages and a stitching procedure is used to correct translation effects (tilts) and to reconstruct the surface profile.
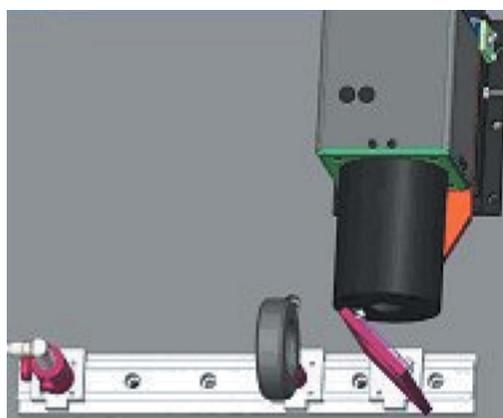
In this article we present the development of a Shack–Hartmann measuring head (SH-LTP head) specially designed to be embarked on a LTP translation stage long-trace profiler. The SH-LTP head is built around a high-sensitivity, high-accuracy and high-dynamic-range Shack–Hartmann sensor. In the second part of the article a description of the instrument is given and its performances are presented. In the third part the experimental validation of the instrument is performed with the characterization (for the Soleil synchrotron) of an X-ray toroidal mirror. The results are compared with measurements made with Soleil's LTP in its standard measuring configuration which has been fully cross-checked with similar instruments of other synchrotron metrology laboratories.

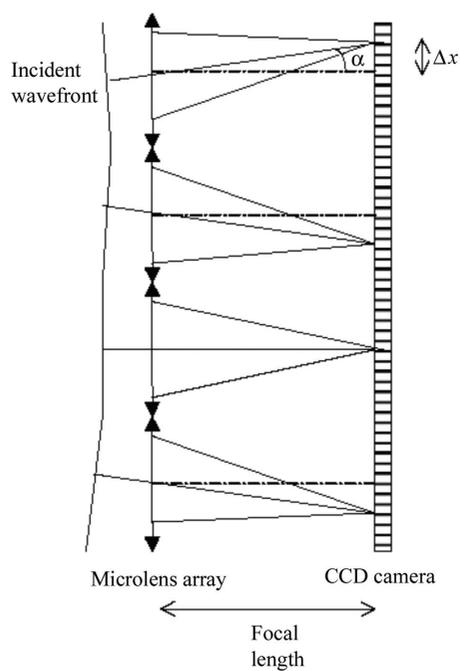## 2. Description and performances of the SH-LTP head

2.1. Description of the SH-LTP head

The principle of the SH-LTP measuring head is as follows. A plane wavefront is sent towards the surface of the mirror to be measured. The reflected wavefront is directed towards the HP26 Shack–Hartmann wavefront sensor (SHWS) from Imagine Optic. A schematic diagram of the profilometric head is given in Fig. 1(a).

The plane wavefront is produced by collimating a single-mode fiber-coupled laser diode emitting at 405 nm with a doublet and is directed towards the surface under test by a 50% beamsplitter at 45°. All components are mounted on an aluminium base plate which can be easily fastened onto the translation stage of Soleil's LTP. It is clear that the collimation of the beam directly influences the accuracy of the system.

(a)

(b)

Figure 1
(a) Profilometric head. (b) SHWS principle.

This is performed by adjusting the distance between the fiber extremity and the doublet so that the sensor measures an infinite radius of curvature. The accuracy and stability of the collimation is very high, typically less than 1 µrad.

The HP26 SHWS is made of a microlens array and a CCD camera located at their focal plane. Fig. 1(b) shows a schematic diagram of the sensor. The microlens array samples the incident wavefront in beamlets; each beamlet focuses on the CCD where an array of spots can be observed. Each microlens (or spot) is identified by two indexes i and j, i being associated with the X axis and j with the Y axis. The centroids of the spots are estimated via a high-accuracy detection algorithm and compared with the reference positions given by a perfect incident beam (Imagine Optic proprietary calibration method). Knowing the displacements in two dimensions of each spot from its reference position enables us to obtain the wavefront local slope at the considered position. For the microlens (i, j), the local slopes are $\alpha_{ij}^x = \Delta x/f$ and $\alpha_{ij}^y = \Delta y/f$, where f is the microlens focal length, and Δx and Δy are the spot displacements. By numerical integration, the wavefront is then reconstructed (Southwell, 1980).

The dimensions of the analysis pupil of the SHWS are 11.7 mm × 11.7 mm. The wavefront sensitivity and accuracy of the sensor is enhanced by choosing a working wavelength as short as 405 nm and by giving a long focal length (80 mm) to the microlenses. This focal length results in a rather large microlens pitch (450 µm). The chosen design uses a microlens array of 26 × 26 square-rotated microlenses. This Imagine Optic patented technology (Imagine Optic, 2002) of square-rotated microlenses decreases the interference effects between adjacent spots by rotating the microlenses through an angle of 25° (thus increasing the accuracy by a factor of two). The detector is an 8-bit megapixel CCD camera with square pixels (12 µm). The sensitivity of the SHWS depends on the centroid position estimation, which is approximately 1/1000 of a CCD pixel. Thus, the sensitivity is 0.2 µrad on local slopes and 0.08 nm on local wavefront error. A spot tracking algorithm strongly improves the dynamic range of the SHWS to the value of ±17 mrad so that spot shifts as large as ±3 microlens pitch are still accurately measured. With this improved dynamic range, wavefront radii of curvature down to 350 mm (i.e. surface radii of curvature of 700 mm) are measurable. The Imagine Optic proprietary calibration procedure ensures the accuracy and the linearity of the SHWS.

2.2. The stitching approach

In order to characterize the whole surface of synchrotron mirrors whose dimensions are larger than the analysis pupil of the SHWS, it is necessary to use translation stages and perform a surface mapping. The translation of Soleil's LTP has a pitch, roll and yaw lower than 10 µrad PV (peak-to-valley) over the whole 1 m-long travel, and the accuracy of the position is better than 5 µm. In the following, we only use a one-dimensional translation stage but the procedure can be

straightforwardly extended from one-dimensional to two-dimensional.

In order to make an accurate surface reconstruction, it is necessary to know the orientation of the SH-LTP head at each step with an accuracy at least equal to the SHWS sensitivity (in the 0.1 µrad range). Invariance of the orientation at this level cannot be ensured by simple mechanical means. But the orientation information should be recovered from neighboring measurements by a stitching technique similar to those implemented in sub-aperture interferometry. This method has been extensively used and its efficiency confirmed (Mimura *et al.*, 2005; Otsubo *et al.*, 1994; QED Technologies, 2005; Raymond *et al.*, 2002; Yamauchi *et al.*, 2003). The measurement is carried out by overlapping adjacent zones. The ratio between the dimensions of the overlapping area between zones and the SHWS pupil is called the coupling ratio. This coupling rat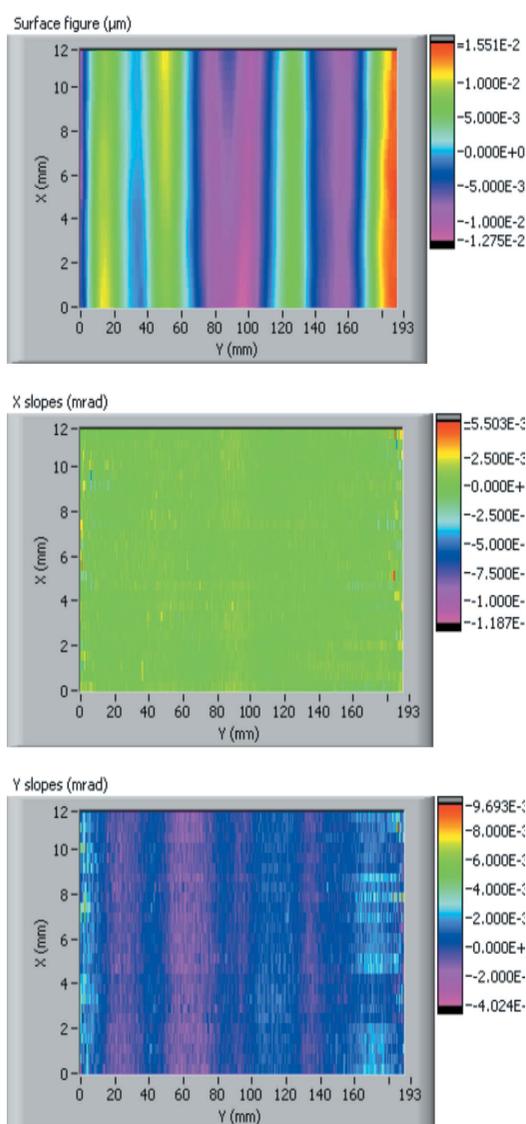io is typically more than 50%. By linearly fitting the local slope differences with a least-square algorithm on the overlapping areas, it is then possible to extract the relative tilts between adjacent zones values and compensate them.

2.3. Calibration of the SH-LTP head: reconstruction of a flat reference surface and comparison with the Soleil LTP result
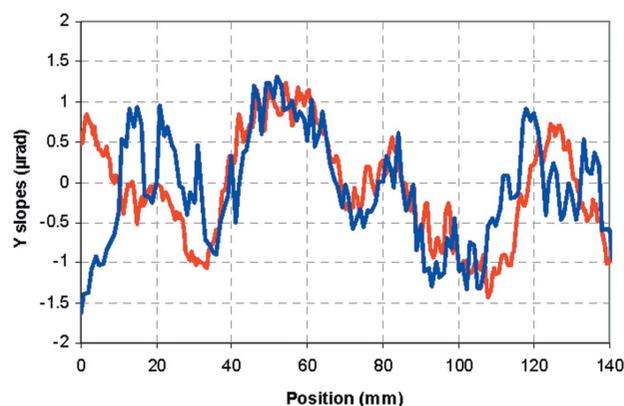
The experimental validation of the SH-LTP head is performed as follows. In a first step it is required to calibrate the SH-LTP head by measuring its systematic error function. This calibration is of prime importance because of the presence of wavefront defects introduced by the SH-LTP head (source, doublet and beamsplitter aberrations). Each measurement made with the SH-LTP head shows two contributions: a static one owing to the head itself (systematic error function) and a dynamic one owing to the surface figure of the surface under test (which varies from location to location). The reference surface for calibration does not need to be perfect. Instead, we use a super-flat reference mirror (with a 200 mm diameter and slope errors of 0.9 µrad RMS over 190 mm and 0.6 µrad RMS over 50 mm) that we measure at different locations and take the average of the measurements (typically 10–20). This averaging drastically smooths the dynamic contribution, then isolating the systematic error function. In a second step we perform a stitching measurement of the reference mirror, taking into account the systematic error function previously determined. The result gives the residual slope error of the mirror and we compare it with the residual slope error obtained with Soleil's LTP.

Stitching results for a 190 mm-long trace with a coupling ratio of 88% are presented in Fig. 2. The surface figure presents a typical low-spatial-frequency pattern for mechanically polished surfaces. RMS and PV errors are 6.9 nm and 28 nm. For X and Y slopes, values of the RMS are 0.61 µrad and 0.99 µrad and the PV errors are 17.4 µrad and 13.7 µrad, respectively. The total number of subapertures over 190 mm is 422 and the measurement time is about 2 min.

Fig. 3 shows a comparison between the SH-LTP head and Soleil's LTP over a 140 mm-long trace. Both measurements

Figure 2
Flat reference mirror over a 190 mm-long trace. From top to bottom: surface figure (28 nm PV and 6.9 nm RMS), X slopes (17.4 µrad PV and 0.61 µrad RMS) and Y slopes (13.7 µrad PV and 0.99 µrad RMS).

Figure 3
Comparison SHLTP-LTP (red curve: SH-LTP; blue curve: Soleil's LTP). SH-LTP: 2.7 µrad PV and 0.66 µrad RMS; LTP: 3.2 µrad PV and 0.72 µrad RMS.

are in good agreement, particularly for the recovery of the low-spatial-frequency pattern. Differences in high-spatial-frequency pattern exist and are due to noise and slight uncertainty in the positions of the traces on the surface (the traces may not be strictly the same). RMS and PV errors are 0.72 µrad and 3.2 µrad for the LTP and 0.66 µrad and 2.7 µrad for the SH-LTP head, respectively.
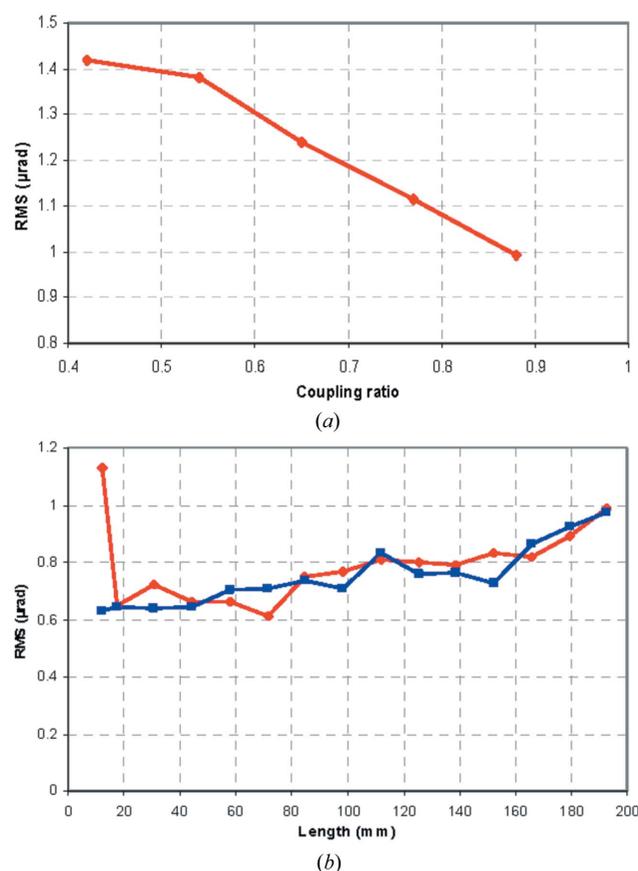
2.4. Stitching performances

The repeatability of the stitching has been measured by performing ten different measurements of the flat reference mirror in the same position. The repeatability is defined as the RMS value of the difference between one of the measurements and the averaging of these ten measurements; thus the repeatability is about 0.1 µrad RMS. This repeatability is 1.5 times better than the repeatability of Soleil's LTP.

The dependency on the length of the trace and on the coupling ratio level of the stitching procedure has been studied with the aid of the reference mirror. In a first step we consider the influence of the length of the trace L (the dimensions of the measured surface are $L \times 11.7$ mm where L is the length of the trace) for a 88% coupling ratio. All traces are symmetric with respect to the center of the mirror (where the surface quality is the better). The result is shown in Fig. 4(a) which represents the RMS slope error of the reconstructed surface for L varying from 12 mm to 190 mm for the SH-LTP head and for Soleil's LTP. We note that the RMS slope error increases quasi-linearly with L in both cases. This linear dependence is mainly due to the surface state of the mirror we explore (its quality is poorer near the edges). In consequence, as both curves are almost identical (particularly for L values of 45 mm, 85 mm and 190 mm where RMS slope errors are 0.65 µrad, 0.74 µrad and 0.95 µrad, respectively) we can conclude that stitching effects are weak. We note that the RMS error passes from 1.13 µrad with one unique zone (11.7 mm × 11.7 mm; no stitching) to 0.65 µrad for the following lengths. This increase in accuracy owing to stitching is a well known effect and is due to the reduction of random noise by data averaging.

Let us consider the influence of the coupling ratio level on the quality of the reconstruction for a 190 mm-long trace. Fig. 4(b) shows the result for coupling ratios between 40% and 90%. We note that the RMS slope error is compatible with the specified value for coupling ratios >85%. In conclusion, submicroradian performances can be achieved with strong coupling ratios.

3. Characterization of an X-ray toroidal mirror

In this section we present some experimental results for a toroidal mirror whose dimensions are 110 mm × 25 mm. Its specified tangential and sagittal radii are 22.2 ± 0.2 m and 0.885 ± 0.015 m, respectively, and its specified tangential and sagittal slope errors are 5 µrad RMS and <15 µrad RMS.
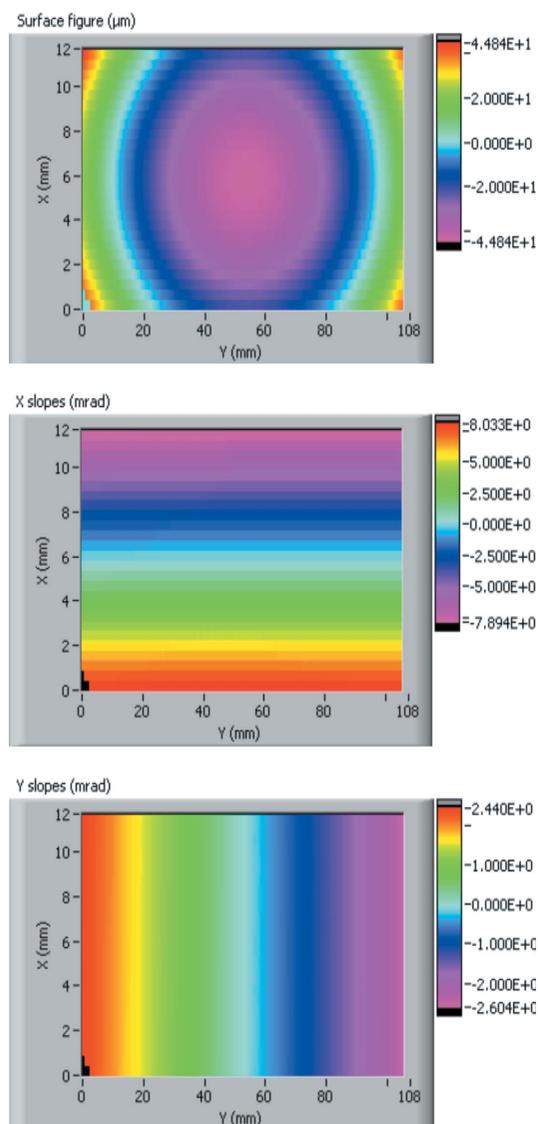

(a)

(b)

Figure 4
Stitching performances in terms of the RMS slope error (a) versus the length of the trace for a 90% coupling ratio (red curve: SH-LTP head; blue curve: Soleil's LTP), and (b) versus the coupling ratio for a 190 mm-long trace.

This mirror has been measured with a coupling ratio of 88%, i.e. adjacent zones are shifted by 3 microlens pitches.
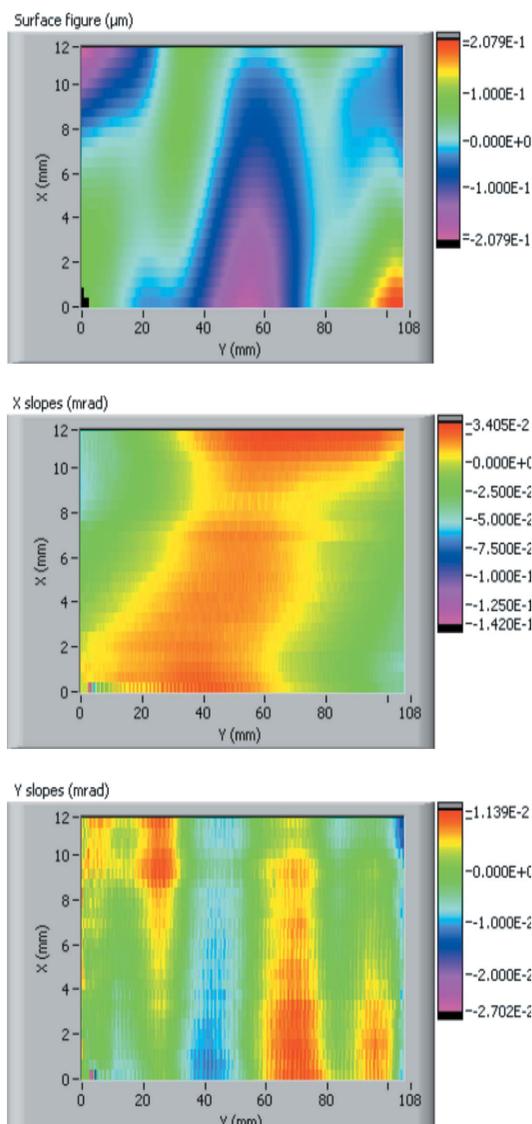
3.1. Toroidal mirror in tangential position

In a first step, the measurement is performed along the largest dimension corresponding to the tangential radius. The alignment of the axis of the mirror with the translation axis is optimized by minimizing the 45°-astigmatism Zernike coefficient. This optimization procedure is very easy to implement by dynamically visualizing the Zernike coefficients on the SHLTP-LTP software. This constitutes one of the major advantages of the SH-LTP head over LTPs, for which the orientation of the mirror is performed by maximizing or minimizing (depending on the position of the mirror) the measured radius of curvature by trial and error.

Fig. 5 represents the stitching result for a 110 mm × 12 mm analysed surface where we clearly recognize astigmatism (owing to the toroidal shape). We can see from this figure the large dynamic range of the SH-LTP head: 89.7 µm PV, 15.9 mrad PV and 5.04 mrad PV for the shape, X slope and Y slope, respectively. The radii of curvature are obtained by fitting the X slopes and the Y slopes to the equation of a plane ($ax + b$ and $cy + d$ for X slopes and Y slopes, respectively, where b and d are the tilts, and $1/a$ and $1/c$ are the radii of

Figure 5
Toric mirror stitching result in the tangential position. From top to bottom: surface figure (89.7 µm PV and 21.3 µm RMS), X slopes (15.93 mrad PV and 4.74 mrad RMS) and Y slopes (5.04 mrad PV and 1.45 mrad RMS).

Figure 6
Toric mirror stitching result in the tangential position after subtracting the best toric shape. From top to bottom: surface figure (416 nm PV and 74.6 nm RMS), X slopes (176 µrad PV and 18.9 µrad RMS) and Y slopes (38.4 µrad PV and 5.67 µrad RMS).
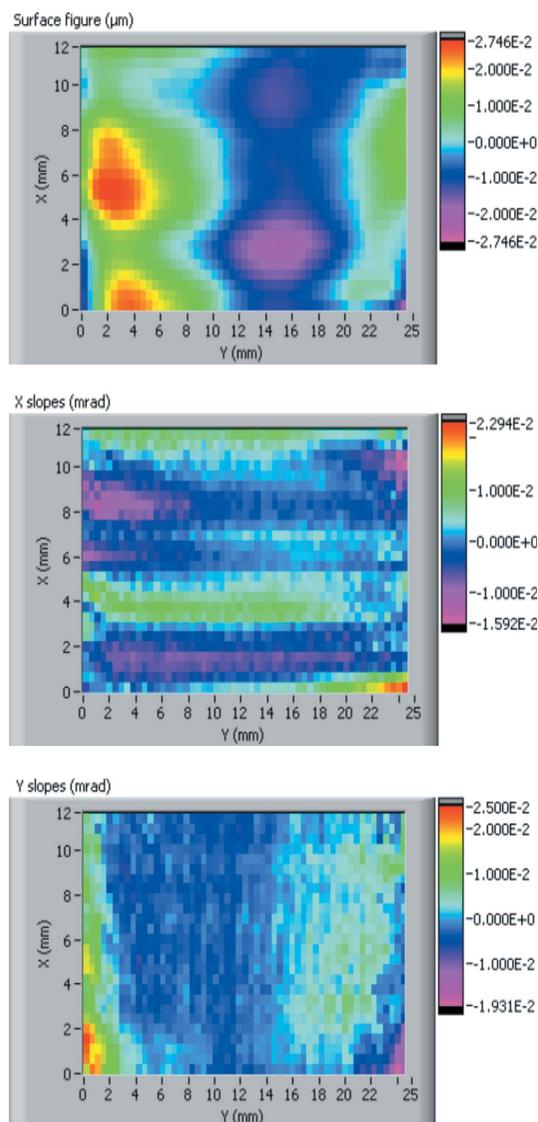
curvatures along the X and Y directions). Thus, the radii of curvature are 22.132 m and 0.879 m, in very good agreement with the specified values. The slope and shape polishing errors are calculated by a least-squares difference with the best toroidal fit (astigmatism filtering). The results are given in Fig. 6. RMS errors on shape and slopes are 74.6 nm, 18.9 µrad (X slope) and 5.67 µrad (Y slope) and PV errors are 416 nm, 176 µrad and 38.4 µrad respectively. We note the presence of a high-frequency pattern. This pattern may have different origins: high-frequency pattern of the surface figure, noise and possible small stitching effects. According to the manufacturers, the first contribution is the most important because the polishing process for toroidal surfaces is far less effective than for flat surfaces, resulting in a slightly deteriorated surface figure. Stitching effects and distortion effects (which are negligible for flat surfaces) might contribute in the case of

highly curved mirrors whose radii of curvature are near the dynamic range limit of the system, but this contribution remains small.

3.2. Toroidal mirror in sagittal position

The analysed surface is 25 mm × 12 mm. It is important to note that characterization in the sagittal position is impossible with the LTP because it lacks the curvature dynamic range.

Fig. 7 represents the result of the stitching after subtracting the best toroidal fit as above. RMS errors on shape and slopes are 11.9 nm, 3.59 µrad (X slope) and 4.07 µrad (Y slope). PV errors are 54.9 nm, 38.9 µrad and 44.3 µrad, respectively. Again, a high-frequency pattern whose origin is the same as indicated above is observed.

Figure 7
Toric mirror stitching result in the sagittal position after subtracting the best toric shape. From top to bottom: surface figure (54.9 nm PV and 11.9 nm RMS), *X* slopes (38.9 µrad PV and 3.59 µrad RMS) and *Y* slopes (44.3 µrad PV and 4.07 µrad RMS).

4. Conclusion

We have demonstrated that a Shack–Hartmann head mounted on a LTP translation stage is an efficient set-up for X-ray mirror characterization. Its high flexibility, robustness, compactness and its performances (accuracy in the submicro-radian range, wide dynamic range, bidimensional measurement) make the SH-LTP head a promising complement or alternative to existing technologies such as interferometers and standard LTPs.

SH-LTP applications are diverse: optical/wafer surface figure metrology (with large dimensions and/or highly curved shapes like aspheres, mirrors for space, synchrotron X-ray mirrors *etc.*), post-polishing control and surface local finishing for the industry, simultaneous non-contact measurement of radii of curvature along orthogonal directions (surface astigmatism). A full-automated instrument with two-dimensional translations is currently under development in order to perform two-dimensional mappings of the whole surface of components.

In order to improve the curvature dynamic range, both the inclusion of perfectly calibrated relay optics and the design of a novel Shack–Hartmann sensor are considered.

References

Imagine Optic (2002). Patent PCT/FR02/02495.
Mimura, H., Yumoto, H., Matsuyama, S., Yamamura, K., Sano, Y. & Ueno, K. (2005). *Rev. Sci. Instrum.* **76**, 045102.
Otsubo, M., Okada, K. & Tsujiuchi, J. (1994). *Opt. Eng.* **33**, 608–613.
QED Technologies (2005). Patent US6 956 657 B2.
Raymond, T. D., Neal, D. R., Topa, D. M. & Schmitz, T. L. (2002). *Proc. SPIE*, **4809**, 208–216.
Southwell, W. H. (1980). *J. Opt. Soc. Am.* **70**, 998–1005.
Thomasset, M., Brochet, S. & Polack, F. (2005). *Proc. SPIE*, **5921**, 12–20.
Yamauchi, K., Yamamura, K., Mimura, H., Sano, Y., Saito, A. & Ueno, K. (2003). *Rev. Sci. Instrum.* **74**, 2894–2898.